Battery Cooling Simulation using STAR-CCM+

Daniel Grimmeisen[1], Marc S. Schneider[1]

[1]CASCATE GmbH

1 Abstract

A generic Li-ion battery pack as typically used in an electric vehicle is simulated in STAR-CCM+, using an analytical model for the electrochemical battery behavior and a thermal/flow simulation with conjugate heat transfer to determine the cooling efficiency. A single Li-ion battery cell is modeled in Battery Design Studio. This model is then used in the Battery Simulation Module of STAR-CCM+, which allows to embed the cell within an electric circuit and to put it under a prescribed load. The battery model then calculates the heat development in the cell based on the load and the electrochemical model. This heat is applied as a distributed heat source in the fluid simulation, which can then be used to investigate and optimize the cooling efficiency.

2 Introduction

Between 2013 and 2018, worldwide electric car stock has grown from under half a million vehicles in 2013 to over 3 million [1] in 2018. Together with the United States and China, Europe is the third of the three big contributors to the global demand of electric vehicles. In Germany, electric car sales have increased by 121% between 2016 and 2017 [1]. This shows the potential in business opportunities for European companies. One of the industry's main challenges is the range of these vehicles, which is limited by battery capacity. Therefore, development of high-capacity high-power battery cells is of the utmost importance for the future success of electric vehicles. Currently, rechargeable lithium-ion battery cells are used by the broad majority of car manufacturers.

To achieve the highest possible longevity of the batteries while at the same time offering high power output during everyday use, it is important to carefully regulate the temperature. High and low temperatures are both unfavorable for the battery's performance so a cooling system has to be added.

Conducting experiments on the heating of batteries when exposed to a prescribed load offers, to some extent, insight on how a battery cooling system performs. However, this method has certain drawbacks. Design optimization is tedious, because every change in geometry requires a new physical model. Additionally, measurements are difficult and feasible only for few points of interest. Measuring can also influence the system, e.g. impose turbulence on the laminar flow of a low velocity cooling fluid. Lastly, long-term experiments on the aging of a battery and subsequent change in its heat distribution take years to finish.

An alternative to experiments is numerical simulation, where the physical properties of the batteries and the cooling system are translated into a computer model that can run the same tests digitally. With that, design changes can be implemented fast, the simulation can be probed at any given point and for any given physical quantity, and year-long experiments can be calculated in a matter of minutes to days. Numerical simulation within this work is conducted in Simcenter STAR-CCM+, a CFD-focused multiphysics simulation software originally developed by CD-adapco. Since 2017, it is owned and distributed by Siemens PLM Software. Centered around fluid dynamics, its core competencies also include multiphase flows, reacting flows, heat transfer, electrochemistry, electromechanics, solid mechanics and rheology [2].

To model the battery cell, Battery Design Studio (BDS) is used. This software was originally developed by Battery Design LLC which in 2009 was acquired by CD-adapco. In BDS's environment, both physical behavior as well as geometric properties of a battery are designed. Also, the battery's performance can be analyzed [3]. The designed battery cell is then integrated into STAR-CCM+. There, not only cell performance is simulated, but also thermal behavior as well as further interactions with surrounding bodies.

This test case focuses on the thermal heating of a lithium-ion battery module consisting of sixteen cells. Also, it includes cooling of said module by an attached cooling channel. Water is used as the cooling fluid. The occurring heat transfer mechanisms are modeled in STAR-CCM+. Heat conduction is considered within the battery cells and at the interface between the battery cells and the cooling channel. Forced conduction is simulated in the cooling channel.

3 Electric Vehicle Application

Electric Vehicles nowadays use lithium-ion (Li-ion) batteries to provide energy for the powertrain. Compared to other battery systems, they are lightweight and provide high energy densities [4]. A Li-ion battery consists of a positive electrode, called cathode, and a negative electrode, called anode. They are separated by a polymeric membrane to avoid short circuits. The electrodes are also contacted by an electrolyte containing lithium ions that can pass through the microporous polymeric membrane. Electrons however are kept from passing the membrane. When charging, the ions internally move to the anode while on discharging, they move to the cathode. This is called the *shuttle chair* mechanism [5]. The setup is shown in Fig.1. Various materials can be used for cathode and anode. They differ in their electrode potentials and have different strengths and weaknesses that come with the characteristics of the materials. Research on Li-ion batteries has led to doubled capacity in the 15 years between 1995 and 2010 [6] with the potential to double again until 2025.

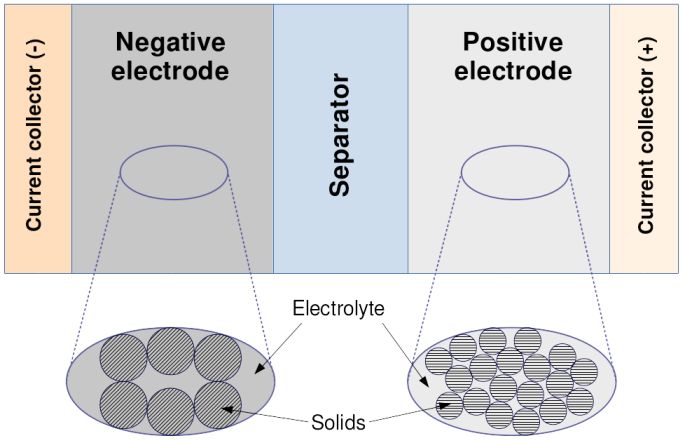

Fig.1: Li-ion battery cell with three regions and two phases (adapted from [7])

Li-ion batteries can have different designs. For an electric vehicle application, usually either cylindrical cells or pouch cells are used. Multiple cells are connected to form a module. Multiple modules are connected to form a pack that is then built into the vehicle. Packs are designed to fit into the available space and to comply with vehicle requirements such as size, power and voltage [6]. Also, the pack includes sensors and a controller to regulate cooling and charging/discharging current. Fig.2 shows the model of a typical pouch cell as it is used in this test case. On the top left are the tab connectors to connect battery cells to one another.

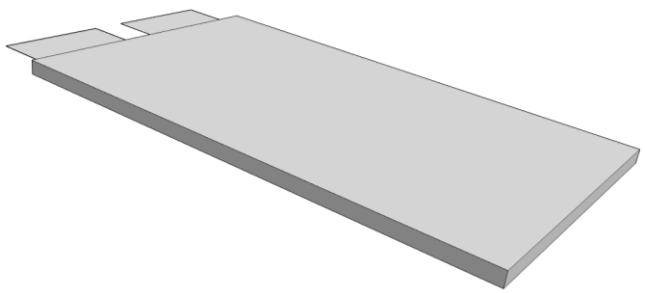

Fig.2: Pouch battery cell with tab connectors

Car manufacturers use different batteries for the different market segments they want to place the car model in. Table 1 shows typical performances of current electric vehicles.

	Audi e-tron	BMW i3	Chevy Bolt	Tesla X P90D
Year	2019	2016	2017	2016
Battery Capacity [kWh]	95	33	60	90
Max. Power [kW]	300	125	150	396
Consumption [kWh/100km]	24.6 [10]	12.6	~13	17.3
Range [km]	400	300	~400	467

Table 1: Typical performances of different battery electric cars [8,9]

4 Physical properties of the test model

The main goal of this work is to use an academic example to investigate the feasibility of battery and cooling simulation in STAR-CCM+. Thus, a test model has to be created that (1) uses battery cells that are exposed to an electric load so they discharge and heat up and (2) uses a cooling channel to transport that heat away from the cells.

To account for (1), a battery cell is created in Battery Design Studio. Its main specifications, as listed in Table 2, should be close to battery cells as used in electric vehicles (compare [11,12]). The specifications are generated in BDS with data on materials and battery cell setup.

Size (without connector tabs)	153mm x 90mm x 4.375mm
Cell Capacity	10.03 Ah
Energy Content	36.7 Wh
Cell Voltage	3.66 V

Table 2: Specifications of the battery cell used in this test scenario

A lithium nickel manganese cobalt oxide cathode is used. It offers high specific energy with low internal resistance on the positive electrode. Graphite is used as the anode. It has good Li-ion transport properties and a high gravimetric capacity [6].

In electric vehicles, battery cells are organized in modules, each consisting of a predefined number of cells. Cells in modules can be patched in series or in parallel [13]. For example, for their Audi e-tron, Audi uses “36 cell modules, each with twelve pouch cells” [8]. For this test case, one module with 16 pouch cells is built. It is assumed to not be necessary to simulate more than one module, since modules should behave comparably to one another if subjected to the same load. The sixteen cells are stacked adjacently. Every other cell is flipped to enable easy wiring of the + and – tabs of neighboring cells. It is possible to simulate tab connectors like wires or welds in STAR-CCM+. This allows to factor in ohmic heating in wires or other connectors. However, for this simulation, connection between cells is only established virtually. The battery’s temperature at rest is set to 290 K.

High temperatures have unfavorable effects on lithium-ion batteries, both in the short term as well as in the long term [9]. This makes cooling of car battery systems inevitable. In this test, a cooling channel is set up to transport heat away from the batteries. The profile is chosen to be rectangular, with the longer side (1 cm) attached to the side walls of the batteries and the shorter side (3 mm) perpendicular. The channel is looped, so that more heat can be absorbed by the flow. Water is used as a cooling liquid and the flow speed at the inlet is set to 0.3 m/s. Initially, the temperature of the flow is set to 290 K and its pressure is set to 1 bar. Fig.3 shows the test geometry. The sixteen battery cells are stacked, the + and – tabs are facing upwards. Marked in red is the inlet of the cooling channel.

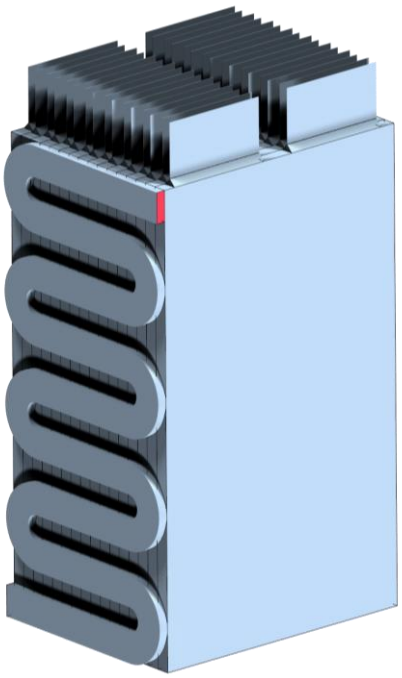

Fig.3: CAD model of the test setup consisting of 16 battery cells and a cooling channel

A charge-discharge cycle has to be developed to apply a load on the battery module. To emulate a driving car, the discharge current is set to 60 A over the course of four minutes. After that, the battery will rest for six minutes to allow it to cool down. The discharge power can be calculated with $P = U \cdot I$. For a single battery cell, a 60 A load leads to a discharge power of 220 W ($U = 3.66\ \mathrm{V}, I = 60\ \mathrm{A}$). A module consisting of 16 serially wired cells therefore has a discharge power of $16 \cdot 220\ \mathrm{W} = 3.5\ \mathrm{kW}$.

5 Numerical treatment of the test model

Two models are used to numerically assess the battery cells: (1) The behavior of the electrolyte within the cell is described with the *General Electrolyte Model*. This model calculates diffusive ion transfer in the electrolyte. The diffusive coefficient is calculated using a form of the Arrhenius equation and is a function of cell temperature. Required material parameters like conductivity, density and heat capacity have to be provided as either constant values, polynomials or data tables. (2) The electronic and thermal behavior is covered by the *NTGPTable* model. This model approximates batteries as a voltage source and a resistor wired in series. Experimental assessment of batteries at fixed states of charge gives the dependency of voltage and current density. This data is then plotted and interpreted to derive the parameters for the model voltage source and the model resistor. The parameters are written in a table and are subsequently fit to a Bezier spline. The model also considers loss of capacity at higher charge/discharge rates [14]. These models are set up in Battery Design Studio before exporting the battery cell to STAR-CCM+.

Physical processes rely on conservation equations that have to be met at every point in space and time. Three of the fundamental conservation equations regard mass, energy and momentum. Being partial differential equations, they have no analytical solution without simplification. When solving complex problems, simplifying the equations is not possible, so they have to be approached numerically. To do that, the conservation equations are put in a form that can be evaluated numerically. Various methods exist to achieve that but most fluid dynamics solvers rely on the finite volume method. For that, the computational domain is spatially discretized by a mesh and temporally discretized by definition of a time differential that the solution advances with. The differential terms of the integral form of the conservation equations are then discretized and the flux over the boundaries of every spatially discretized cell is calculated [15].

On the computational domain, two unstructured meshes of polyhedral cells are created. The first of the two meshes extends over the batteries and the tabs. It consists of approx. 300000 cells that have a base size of 5 mm. The thin areas near the connector tabs have a finer mesh with a base size of 0.625 mm. The second mesh covers the cooling channel. It consists of approx. 500000 cells with a base size of 0.5 mm. The mesh in the boundary layer is refined with prism cells. The grid resolution in the cooling channel (maximum wall *y+* is 2, average wall *y+* is 0.6) is chosen in order to have sufficient data for the evaluation of the narrow channel's cross-section. The cooling channel mesh has an inlet and an outlet. The inlet is modeled as a velocity inlet with a specified velocity magnitude perpendicular to the boundary plane, the outlet is modeled as a pressure outlet with a specified pressure.

For the implicit temporal discretization a time step of 1 s is used. A smaller time step is not necessary because processes in the battery are slow and velocities in the cooling channel are small. A lower time step increases the system's stability since the flow will not advance as much during one time step. A time step of 1 s allowed the simulation to be stable at all times while still being coarse enough to allow for a simulated time of 10 min at reasonable computational expense.

The battery cell is included in the simulation by the Battery Simulation Module (BSM), which uses the imported battery cell to form a battery module, place it in a circuit and calculate thermal and electrical behavior of that module [16]. BSM is seamlessly coupled with the other models of STAR-CCM+. This means that cooling of the battery will have an effect on its electrical output and vice versa. To form a circuit, the sixteen pouch cells are connected serially. The + tab of the first cell and the – tab of the last cell are connected to the predefined program file that holds data on the prescribed time dependent loads. The battery cells heat up as a result of the load and act as distributed heat sources for the cooling channel. In the cooling channel, heat is transported away.

Since both the fluid velocity as well as the hydraulic channel diameter are small, the flow will behave mostly laminar (Reynolds number *Re* = 1550 in terms of the hydraulic diameter). However, to cover turbulent effects, the k-ω-SST model is used. This model adds two additional equations for the turbulent kinetic energy k and for the turbulent frequency ω [16]. The cooling efficiency can be maximized if the flow in a cooling channel is turbulent. In a turbulent flow, mixing processes occur due to velocity fluctuations perpendicular to the flow direction. That way, heat is removed from the channel walls quicker, increasing the capability of the flow to absorb heat.

6 Heat Transfer

There are three basic types of heat transfer: (1) conduction, (2) convection and (3) radiation [17]. In this test case, the effect of radiation is neglected because it is assumed to transfer little energy compared to the other two mechanisms.

In (1) conduction, heat is transported via diffusive forces between molecules whereby the molecules are not transported. If heat is applied to a molecule, it vibrates with higher energy than the surrounding molecules. Due to intermolecular interactions, energy is then transported in the direction of the steepest gradient [17]. In a one-dimensional case, this can be expressed with *Fourier's law of heat conduction* that relates heat flux q and temperature gradient $\mathrm{d}T/\mathrm{d}x$ as $q = -k \cdot \mathrm{d}T/\mathrm{d}x$. k is a proportionality constant called thermal conductivity that is dependent on the material. In a one-dimensional rod with different temperature boundaries on both sides, the temperature distribution becomes linear between the boundaries [18]. Usually, conduction occurs in solid materials in which translatory motion is not possible for molecules. In this test case, conduction can be observed within the battery module. Heat is generated to equally be distributed over the volume of the cells. It is then conducted to the side wall where the cooling channel is attached. On that side wall, temperature is lower compared to the battery cell due to the cooling channel, leading to a temperature gradient and heat flux.

If heat is transported via mass transfer, that effect is called (2) convection. This is often connected to buoyancy, because warmer fluid regions have a decreased density and move against the direction of gravity [17]. This is referred to as natural convection, because the fluid motion is generated solely internally by density gradients. If the mass transfer of the fluid is generated by external sources, it is referred to as forced convection. In this test case, the heat transfer within the cooling channel is dominated by forced convection. The effect of gravity is neglected.

In this test case, the cooling channel wall between the channel and the batteries are subject to two conversing heat transfer processes. Heat is applied by the battery cells, but it is also removed by the cooler flow. The temperature of the wall is thus higher than the temperature in the fluid. This leads to a thermal boundary layer in addition to the velocity boundary layer that is inherent near a wall in practically any flow. The temperature profile of such a boundary layer is depicted in Fig.4. T_∞ is the temperature in the free stream, whereas T_W is the temperature of the wall. δ' is the local thickness of the thermal boundary layer.

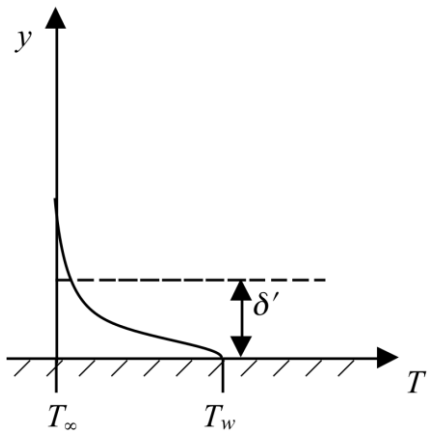

Fig.4: Thermal boundary layer alongside a warm wall [18]

7 Results

The simulated time was ten minutes and the simulation took nine hours to complete with an eight core processor. Fig.5 shows battery and cooling channel temperatures as well as the battery's state of charge (SOC) over the course of the regarded time frame. The SOC starts at 92 % and decreases linearly to 43 % over the first four minutes, during which a constant load is applied to the battery module. Simultaneously, both the average temperatures in the battery module and in the outlet of the cooling channel rise. Both temperatures are 290 K at t = 0s. The temperature in the battery module peaks at 316 K, the temperature in the cooling channel peaks at 299 K, both immediately before the load is removed from the batteries. The temperatures rise faster in the beginning than before cutting off the load. This is because they continue to approach thermal equilibrium, at which as much heat is generated as is transported away by the fluid. Once the load is cut off, temperatures asymptotically approach the initial conditions again.

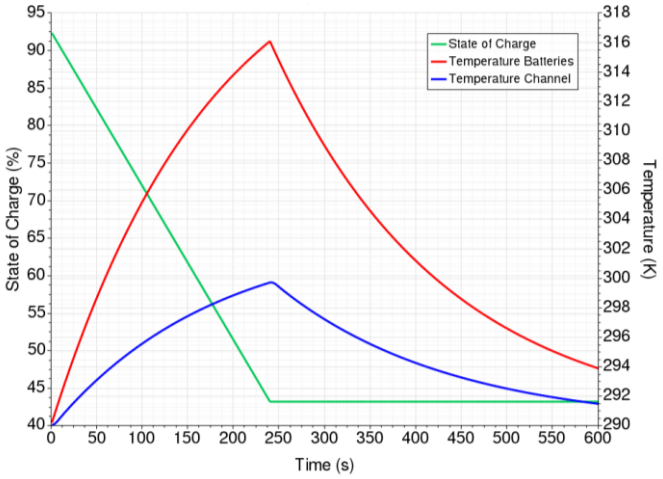

Fig.5: Time-dependency of SOC and temperatures in batteries and cooling channel

A closer look at the battery cells reveals a sub-cell structure as can be seen in Fig.6. As expected [16], the battery cell has the highest heat generation near the tabs (not shown). Close to the cell walls, heat

generation drops to almost zero because no chemical reactions take place there. The volumetric heat distribution is qualitatively time-independent, but absolute values decrease by 3% between t = 0s and t = 240 s while the SOC decreases.

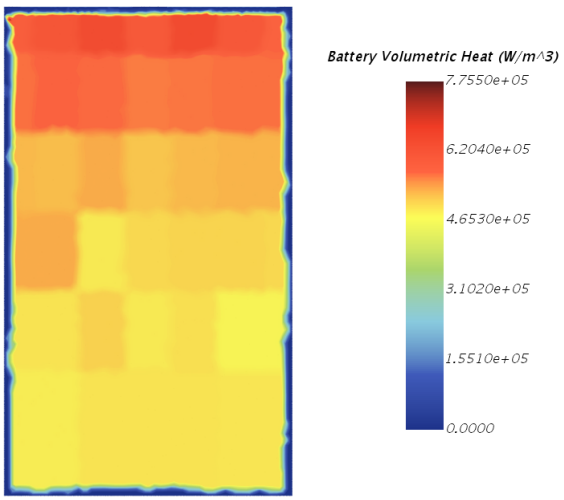

Fig.6: Volumetric heat generation of a single battery cell when subjected to a discharging load

However, the distribution of generated heat on the surface of the battery cell has only little influence on the temperature distribution of the battery module. This is shown in Fig.7. With the mechanisms of heat transfer as explained in Ch.6, heat is transported away from the regions of highest generation. This means it spreads both directed towards the bottom of the module, where less heat is generated, and also towards the cooling channel where it is then transported away by the fluid. It can be noticed that the fluid in the cooling channel heats up between the inlet on the top right side in Fig.7 and the outlet on the bottom left side.

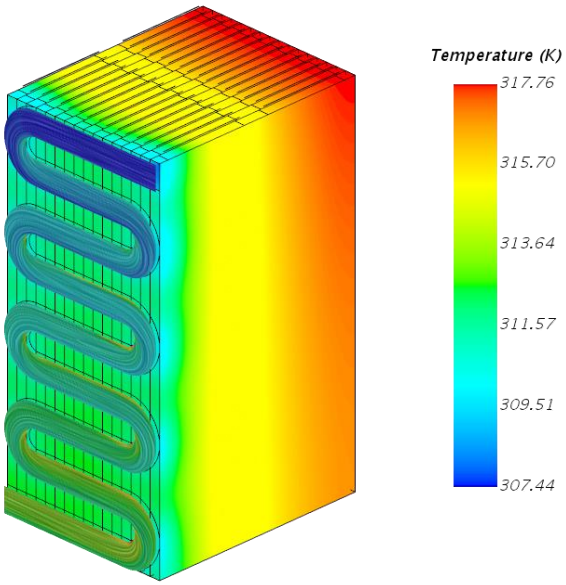

Fig.7: Temperature distribution on the battery module and the cooling channel at t = 240 s

The heat flux that passes the boundary between the battery module‘s wall and the cooling channel is depicted in Fig.8. The inlet is located in the top left corner, the outlet in the bottom right corner. The absorbed heat of the flow is generally higher in the areas where the channel turns. Here, mixing processes due to the change of direction of the flow disturb the boundary layer which isolates the free stream from the wall. This might be a result of secondary flow, a minor flow field that is superimposed

over the primary flow [19]. In Fig.8, the effect of secondary flow can be observed at the recurring patterns of high boundary heat flux at the turns of the cooling channel.

Also, more heat is added to the fluid closer to the inlet compared to closer to the outlet. While flowing through the channel, the fluid‘s temperature constantly rises, lowering the temperature difference between the battery module‘s wall and the fluid. According to *Fourier’s law of heat conduction,* this results in less added heat.

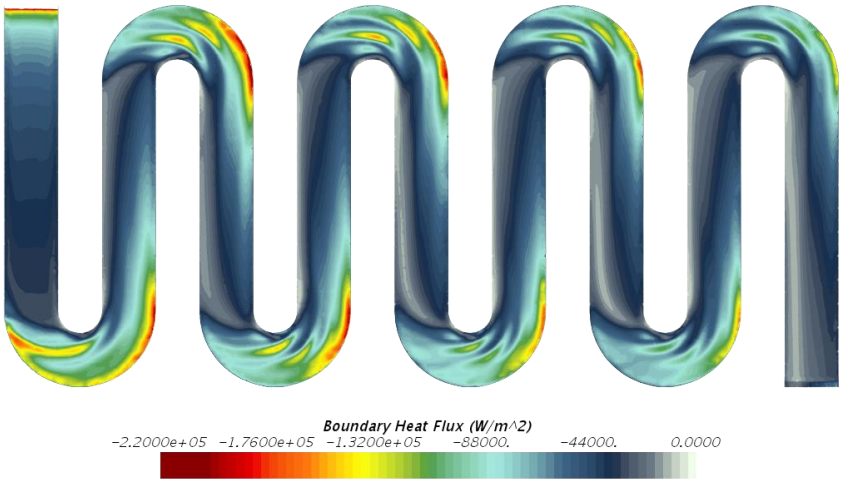

Fig.8: Heat flux over the boundary between the battery module and the cooling channel at t = 240s

The time dependency of the average heat flux that is transferred from battery module to channel is shown in Fig.9 in comparison to the average temperature of the battery module. Temperature and heat flux show good agreement. This means that all heat that is generated in the module is transported away by the cooling fluid. Due to the setup, where all outside walls of the geometry are considered adiabatic, heat can only move towards the channel where it is then transported away.

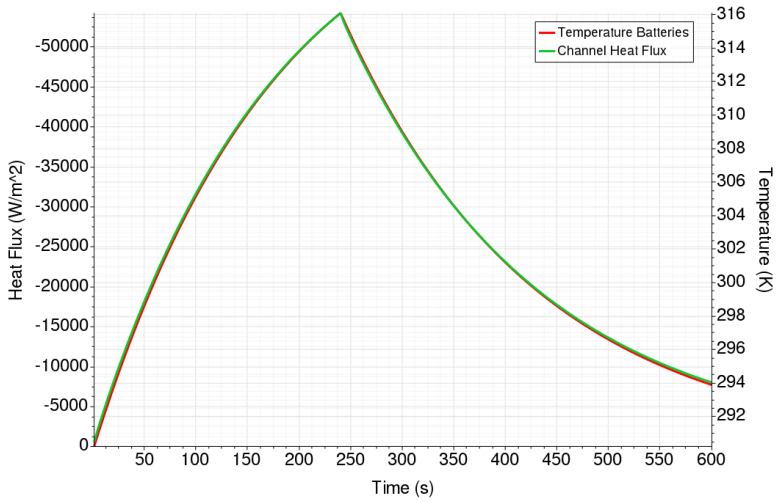

Fig.9: Time-dependency of average battery temperature and average heat flux into cooling channel

Because of the lower temperature of the cooling fluid in comparison to the battery module wall, a thermal boundary layer exists near the wall of the cooling channel, as explained in Ch.6. This is shown in Fig.10. This plot is created at t = 240 s, so the temperature in the battery module is at its peak. The profile is taken at the outlet. The temperature on the battery module‘s wall is 311.3 K. The thickness of the thermal boundary layer as compared to the velocity boundary layer is given by the Prandtl number *Pr*. A Prandtl number of 1 means that both boundary layers have the same thickness. For the conditions in this test case, the Prandtl number is *Pr* = 7.7 (interpolated, [20]). This means that the thermal boundary layer is thin, which is beneficial for cooling purposes.

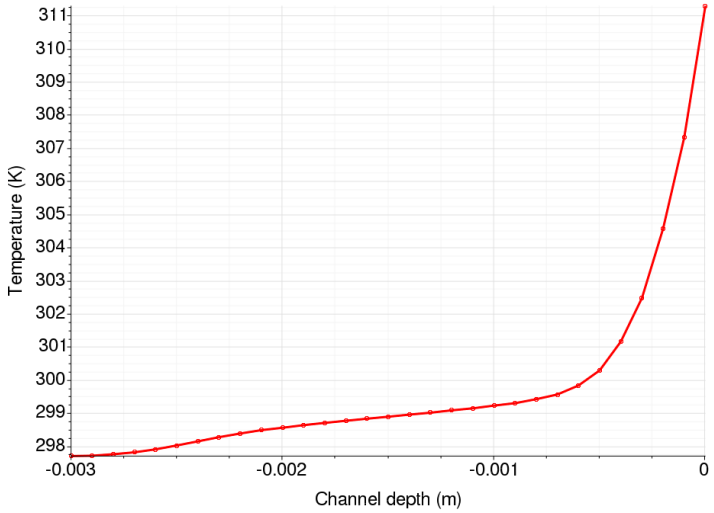

Fig.10: Temperature profile at the outlet of the cooling channel wall at t = 240s

8 Summary

In this work, a test case has been set up to model the cooling of a battery module that is subjected to a discharging load. For that, a battery cell was designed in Battery Design Studio to meet the requirements of modern electric vehicles. Both geometric properties as well as chemical processes were specified in BDS. After that, the battery cell was imported into STAR-CCM+. A battery module consisting of sixteen battery cells was created, with the cells wired serially. The resulting circuit was loaded with a discharge cycle in which a current of 60 A was applied for 240 seconds, during which the state of charge of the battery module decreased from 92 % to 43 %.

The chemical reactions taking place within a battery cell during charging and discharging produce heat that is unfavorable for long-term and short-term performance of the cell. Thus, cooling was considered in this test case. A cooling channel was created with the 3D-CAD-module of STAR-CCM+. It was designed so that it passes all battery cells to absorb heat and to cool the cells. Water was used as the cooling fluid. The Reynolds number of the flow in the channel was Re = 1550 and the Prandtl number was Pr = 7.7. Thus, although the flow was mostly laminar, the cooling effect of the fluid was good because the thermal boundary layer was small and heat could be transported to the free stream efficiently.

The heat distribution of the battery cells, the temperature distribution of the battery module, the heat flux between the battery module and the cooling channel as well as the thermal boundary layer were investigated. It was shown that both the simulation of the behavior of the batteries as well as the simulation of the conjugate heat transfer and subsequent transport of heat are feasible in STAR-CCM+ with little computational expense. Thus, more complex cases can be set up to numerically assess current battery pack designs and to advance battery technology by facilitating the design process in all associated industries.

9 Literature

[1] International Energy Agency Publications: “Global EV Outlook 2018”, 2018
[2] CD-adapco: “STAR-CCM+ ENGINEERING DISCIPLINES”, 2016
[3] CD-adapco: “CD-adapco + Battery Design LLC = New Battery Simulation Technology”, 2017
[4] Tarascon, J.-M. and Armand, M.: “Issues and challenges facing rechargeable lithium batteries”, Nature 414, 2001, pp. 359-367
[5] Deng, D.: “Li-ion batteries: basics, progress, and challenges”, Energy Science and Engineering 2015; 3(5), 2015, pp. 385-418
[6] Greenwood, D.: “Automotive Batteries 101”, 2018
[7] Xue, N.: “Design and Optimization of Lithium-Ion Batteries for Electric-Vehicle Applications”, 2014
[8] Lehner-Ilsanker, T.: “The Audi e-tron”, Press Information, 2018

[9] Schüppel, F., Schlüter, M. and Gacnik, J.: “Design of battery electric vehicles in accordance with legal standards and manufacturers’ and customers’ requirements”, Der Antrieb von morgen 2017, 2017
[10] Audi AG: “Technische Daten und Kennwerte: Audi e-tron 55 quattro (265 kW)”, available online, 2019
[11] A123 Systems, Inc.: “Nanophosphate Lithium Ion Prismatic Pouch Cell AMP20M1HD-A”, 2011
[12] Farasis Energy, Inc.: “IMP06160230P25A Rechargeable Lithium-ion pouch cell based on high capacity NMC cathode technology.”, 2011
[13] MIT Electric Vehicle Team: “A Guide to Understanding Battery Specifications”, 2008
[14] Siemens PLM Software: “Battery Design Studio User Guide”, 2018
[15] Munz, C. and Westermann, T.: “Numerische Behandlung gewöhnlicher und partieller Differenzialgleichungen”, 2009
[16] Siemens PLM Software: “Simcenter STAR-CCM+ Documentation”, 2019
[17] Tipler, P. and Mosca, G.: “Physik für Wissenschaftler und Ingenieure”, 6. deutsche Auflage, 2009, pp. 781-783
[18] Spakovszky, Zoltan: “16.050 Thermal Energy”, 2002
[19] Pattison, M.: “Secondary Flows”, 2011
[20] Engineering ToolBox: “Water – Prandtl Number”, 2018